# Intrusion into Granular Media Beyond the Quasistatic Regime

Leah K. Roth,* Endao Han,† and Heinrich M. Jaeger‡
*James Franck Institute and Department of Physics, The University of Chicago, Chicago, Illinois 60637, USA*

(Received 23 October 2019; revised 9 February 2021; accepted 13 April 2021; published 25 May 2021)

The drag force exerted on an object intruding into granular media is typically assumed to arise from additive velocity and depth dependent contributions. We test this with intrusion experiments and molecular dynamics simulations at constant speed over four orders of magnitude, well beyond the quasistatic regime. For a vertical cylindrical rod we find velocity dependence only right after impact, followed by a crossover to a common, purely depth-dependent behavior for all intrusion speeds. The crossover is set by the timescale for material, forced to well up at impact, to subsequently settle under gravity. These results challenge current models of granular drag.

DOI: 10.1103/PhysRevLett.126.218001

Intrusion of a solid object into a static granular medium drives the material beyond yielding and triggers a transformation into a flowing state. Despite stress transmission along irregular, heterogeneous networks that trace out highly nonlinear interparticle contact forces [1–3], the resulting resistance to intrusion can often be described in terms reminiscent of ordinary liquids [4–6]. For sufficiently slow intrusion, in particular, the net force on the intruder resembles an Archimedean law [7,8]. This velocity-independent, quasistatic behavior, where the force $F_z$ is proportional to the depth $z$ below the medium's free surface, forms the basis of many models that predict the resistance to moving through or burrowing into granular material, situations important for animal and robot locomotion as well as for many engineering and geophysical applications [5,9–12]. When the intrusion speed $v$ becomes larger, a term $F_v$ proportional to $v^2$ is added to account for collisional momentum transfer [4,13–21]. As a result, the net force resisting intrusion is typically represented by

$$F(z, v) = F_z(z) + F_v(v^2), \tag{1}$$

Here $F_z \sim z$, with an offset $mg$ if an intruder of mass $m$ enters the granular medium not at constant speed but under gravitational acceleration $g$. $F_v$ is usually assumed to be nonzero only for $v > v_c = \sqrt{2gd_g}$, the speed of a grain falling its own diameter $d_g$ under gravity [22].

However, while these two separate depth- and velocity-dependent contributions to the drag force are used widely, their detailed physical justification has remained debated [4,7,15–17,20,23,24]. Furthermore, whether the contributions are indeed additive has been difficult to test systematically. This is due to a prevalent focus on intrusion under constant force [14,15,20,21,25–27], entangling the depth and velocity dependencies as the impacting object slows and eventually stops.

To isolate these mechanisms, we report on experiments and simulations performed with constant *speed* of intrusion. We focus on dry granular media with sufficiently large particle diameter $d_g$, i.e., permeability ($\propto d_g^2$), that effects due to interstitial air [4,28,29] can be neglected, and on situations where the intruder does not sink through the bed under its own weight [30]. We find that Eq. (1) does not properly represent the behavior of the drag force. Instead, we observe a considerably more complex interplay: the drag force upon contact with the surface is velocity dependent but strongly peaked, and at later times (i.e., larger $z$) returns to the pure depth dependence of the quasistatic limit, even if $v$ exceeds $v_c$ by as much as an order of magnitude.

In our experiments, a flat-bottomed, cylindrical rod with diameter $D = 2$ cm was pushed vertically by a linear actuator (Parker ETT050) into a granular medium, assembled via pouring and composed of glass spheres (Ceroglass, diameter $d_g \sim 2$ mm, density $\rho_g \sim 3$ g/cm$^3$), at a constant velocity $v_0$ that ranged from 0.1 mm/s to 2 m/s [Fig. 1(a)]. The normal force applied by the particles on the rod during intrusion was measured by a force sensor (Dytran 1051V2, Instron 5800) aligned with the rod axis. To visualize the particle dynamics in the interior of the medium during intrusion, the molecular dynamics simulation platform LAMMPS [31] was used to reproduce the experiments as closely as possible [Fig. 1(b)]. For details about the simulations, including validation, variations in $D$ and $g$, and further analysis of flow characteristics, see Ref. [32]. In what follows, we focus on simulations with grains ($d_g = 2$ mm, $\rho_g = 3$ g/cm$^3$) that interact via a frictional Hertzian contact force with normal stiffness $k_n = 10^9$ Pa and friction coefficient $\mu = 0.3$ and that were prepared by pouring under gravity $g = 9.8$ m/s$^2$ with a resulting packing density $\phi_0 \sim 0.61$ [33].

Based on Eq. (1), under conditions of constant intruder speed $v_0$, we would expect all force curves to start at

 

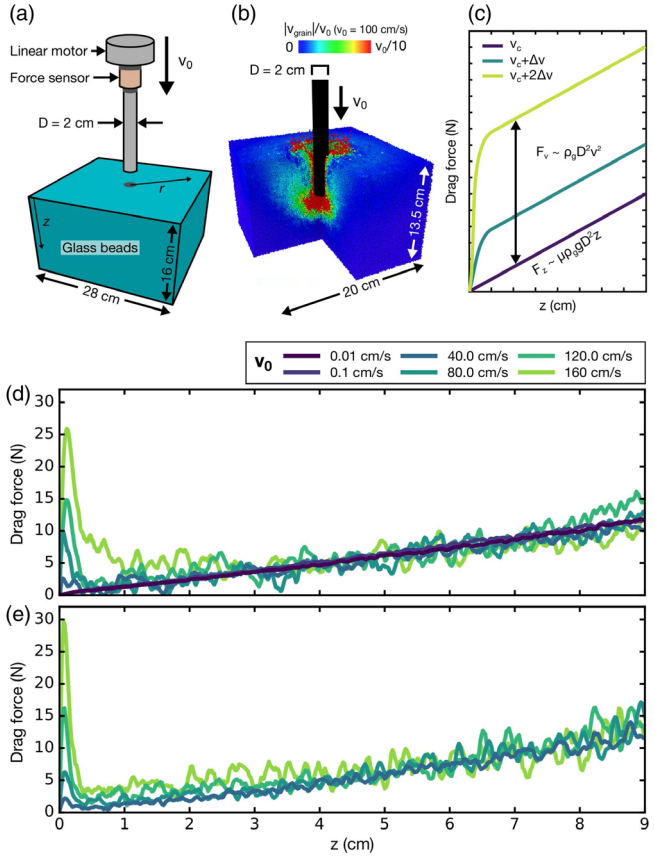


FIG. 1. (a) Experimental setup. (b) Rendered image from simulation. Grains are colored by velocity magnitude ($v_0 = 100$ cm/s). (c) Expected results, based on Eq. (1), for the drag force on an intruder moving at a constant speed $v_0$. (d) Experimental and (e) simulation results for the drag force on a cylindrical intruder as a function of $z$ for different $v_0$.

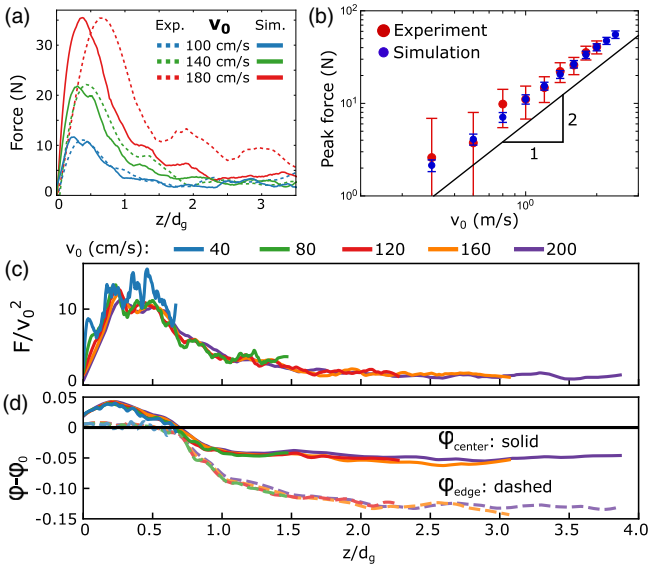


FIG. 2. (a) Force on intruder right after impacting the free surface, as function of intrusion depth $z$ scaled by grain diameter $d_g$. (b) Peak force as function of $v_0$. (c), (d) Normalized drag force (c) and change in packing fraction (d), both from simulations, as a function of $z/d_g$.

$F(v_0, 0) = 0$ and then rapidly transition to a family of straight lines $F(v_0 > v_c, z)$ that are offset parallel to $F(v_0 < v_c, z)$. This is sketched in Fig. 1(c), where we write out the depth- and velocity-dependent contributions in terms of the system parameters, i.e., $F_z(z) \sim \mu\rho_g g D^2 z$ and $F_v(v^2) \sim \rho_g D^2 v^2$.

Both our experiments and simulations, however, show velocity dependence only during the first part of the intrusion, where a sharp peak in force is followed by a brief region of nearly depth-independent drag. All curves then merge onto a common, linear $z$ dependence [Figs. 1(d), 1(e)]. Remarkably, this linear depth dependence remains unchanged while $v_0$ varies over 4 orders of magnitude, extending both below and above $v_c$, where $v_c \sim 20$ cm/s for our granular medium. These results are incompatible with the expected behavior shown in Fig. 1(c) and point to basic physics not captured by Eq. (1).

We first take a closer look at the initial force peak. It occurs as a rapid transient during the first 1–2 ms as the intruding rod penetrates the very top layer of grains [Fig. 2(a); the slight shift in simulated peak position is less than half a grain diameter at the largest $v_0$]. The peak height is proportional to $v_0^2$ [Fig. 2(b)], independent of rod tip shape [34] and consistent with collisional momentum transfer. Scaling $F(v_0, z)$ by $\rho_g D^2 {v_0}^2$ collapses the force profiles for different $v_0$ in this initial phase [Fig. 2(c)].

During the force peak, the average local packing fraction directly below the rod face, $\phi_{\text{center}}$, reaches a brief maximum that is independent of $v_0$ [Fig. 2(d)]. However, once the rod has broken through the first layer of grains, the local packing fraction falls below its original value, resulting in a region of reduced density $\phi_{\text{center}}$ comoving in front of the rod and an even larger reduction at its edge, $\phi_{\text{edge}}$. These results already indicate that the main effect of the initial impact is fluidizing: because $\phi_0 \approx 0.61 > \phi_c \sim 0.59$–$0.60$ for glass spheres, the grains around the face of the rod must dilate to flow [17,27].

A consequence of such fluidization should be an essentially $z$-independent drag force. While not easily seen in Figs. 1(d)–1(e), close inspection of the force curves indeed reveals a short region after the initial peak, where $F(v_0, z)$ is varying little with depth. This is shown in Fig. 3, where we excluded the initial peak and smoothed over the force fluctuations associated with the small $D/d_g$ ratio. The magnitude of the drag force in this region still scales with ${v_0}^2$ [32]. Note that beyond some characteristic depth $z^*$, each of the curves merges onto a common form $F_z = \alpha\mu\rho_g g D^2 z$, with coefficient $\alpha = 35 \pm 5$, behavior usually associated with the quasistatic limit [7,15,20].

From data as in Fig. 3 we find that $z^*$ is directly proportional to $v_0$. Further, fixing $v_0$ but varying $g$ as well

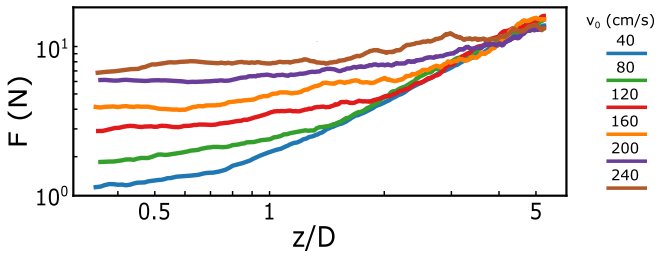


FIG. 3. Force on intruder in fluidized region following the initial peak, as a function of depth $z$ scaled by rod diameter $D$. Data shown are from simulations, smoothed (via moving average, window size $\sim 0.8 d_g$) and with the initial force peak removed. For given $v_0$ this region ends at depth $z^*$ or, equivalently, dimensionless time $\tilde{t} = 1$ (see text) and the force merges onto a common, linear depth dependence.

as $D$ independently to change the ratio $D/g$ by an order of magnitude (see Ref. [32]), we find $z^* = v_0 t^*$, where $t^* = \sqrt{D/g}$. In other words, the crossover to $F_z = \alpha \mu \rho_g g D^2 z$ occurs at a characteristic time $t^*$ that does not depend on $v_0$. For what follows, we therefore introduce a dimensionless time $\tilde{t} = t/t^* = z/v_0\sqrt{g/D}$. That way the crossover from impact speed dependent behavior to purely $z$-dependent drag corresponds to $\tilde{t} = 1$.

To isolate the origin of this crossover, we use the simulations to visualize particle flow fields. The left column of Fig. 4 shows the azimuthally averaged flow as a function of distance $r/D$ from the intruder axis. Three instances are shown (here represented by data for $v_0 = 160$ cm/s): (a) in the initial fluidized regime, (b) at the crossover to the pure $z$ dependence, and (c) inside the purely $z$-dependent regime. In all three cases, the rod is seen to generate intense downward and radially outward flow at its leading edge. In particular, the region of downward flow (negative $v_z$, shown as blue) just ahead of the intruding rod is of characteristic size $D$ and stays roughly constant as the rod moves further into the medium. The most striking qualitative change is found in the vertical velocity component $v_z$ of particles alongside the rod for $r/D \sim 1$–2. There, the flow at first is broadly upward (shown as red) for the full depth of penetration and $v(z)$ at the free surface of the granular medium is positive, signaling an upwelling of fluidized grains [Fig. 4(a)]. At the crossover, the stream lines have begun to bend back towards the rod and there is no longer significant vertical motion at the surface: the top-most grains have begun to settle [Fig. 4(b)]. This settling subsequently serves to isolate the flow around the rod's face and produces an enhanced coupling between the intruder and the bulk, evidenced in Fig. 4(e) by radially far extending flow lines paired with low vertical velocity, in contrast to the high velocity flows in Fig. 4(a). Along with this, the flow at the free surface reverses and grains become entrained and pulled down with the rod. Thus, we can identify $t^*$ with the time at which material near the free surface, which was fluidized and pushed upward during the initial stage of intrusion, begins to settle under gravity.

The three panels in the right column of Fig. 4 demonstrate more quantitatively the change in behavior around $\tilde{t} = 1$ by focusing on the azimuthally averaged velocity profiles $v_z(z)/v_0$ within a region centered at $r/D = 1$ [shown as a vertical gray strip in Fig. 4(a)]. We note, in particular, how $v_z$ at the free surface $z = 0$ crosses through zero at $\tilde{t} = 1$ and becomes negative. Simultaneously, the most intense particle movement, represented by the peak in $v_z/v_0$, becomes more localized and centered around the position of the rod's face (vertical lines).

These results clearly show that $F_v$ is not simply an additive contribution to $F_z$, as implied by Eq. (1). Furthermore, $F_z$ is not linked to the presence of a stagnant zone underneath the intruder as was proposed by Refs. [7,8] and also suggested by Ref. [11] based on observations made in a more confined geometry near a transparent wall. Instead, we identify this as a region of pronounced dilation and shear that interacts with an extensive flow field reaching to the surface of the particle bed (Fig. 3) [23,26,27,35]. Consequently, we find a scenario whereby the intruder dilates, rather than compacts, the medium directly ahead of it, pushing the particles laterally off into the surrounding bulk. This basic scenario does not appear to depend on intruder speed, even when $v_0$ far exceeds $v_c$, the characteristic speed typically signaling the upper limit of the quasistatic regime. Additionally, velocity dependent contributions to the drag force appear only as transient effects near the free surface. As the rod first contacts the surface, collisional momentum transfer results in a brief force peak followed by fluidization of grains in the vicinity of the rod, which causes them to well up against gravity (though these results are specific to a flat rod geometry, see Ref. [34]). Once grains settle down again, after $t^*$, all force curves merge with the quasistatic $z$ dependence. We note that $t^* = \sqrt{D/g}$ also is the time it takes intruders of diameter $D$ that have been dropped under gravity to stop moving inside the medium [16,17]. This supports the idea that the extent of upwelling is set by the initial impact, whether the subsequent intrusion occurs under constant speed, as here, or under constant force.

Given these findings, we expect a change in the behavior of the primary momentum carriers during the transition away from fast mass flux, concentrated near the intruder at early times, to particles moving along much slower but more spatially extended streamlines for $\tilde{t} > 1$. In Fig. 5, we examine grains outside of the direct vertical path of the rod, i.e., for $r > D/2$. In panel (a), we divide these grains into two groups: those whose upward velocity is greater than $v_0/10$, and those with $v_0/80 \geq v_z > v_0/320$ (where $v_0/320$ is the system noise lower threshold). At early times ($\tilde{t} < 1$) the majority of the momentum in the system

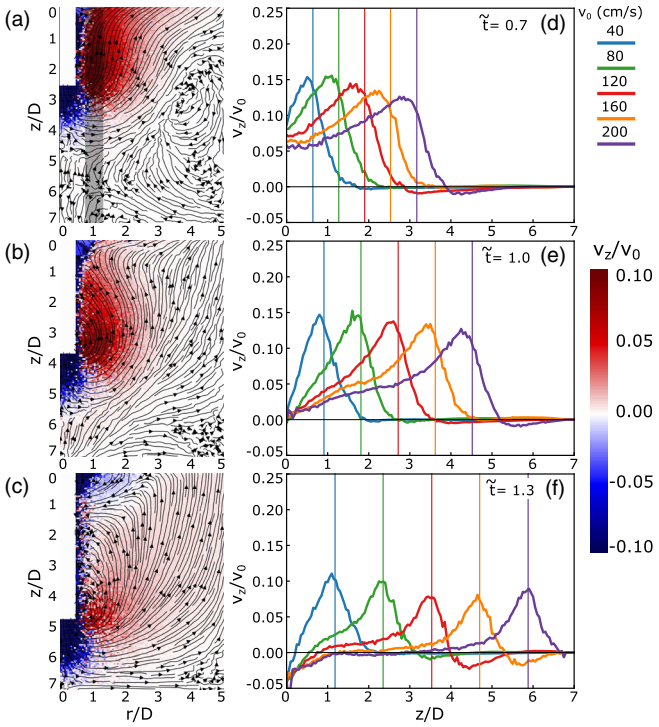


FIG. 4. Simulation results showing flow fields and vertical velocity component $v_z$ at times $\tilde{t} = 0.7$, 1.0, and 1.3 (top to bottom rows). Left column (a),(b),(c): Flow field in the $z$-$r$ plane for $v_0 = 160$ cm/s. Streamlines are shown in black, $v_z$ is indicated by color. The white rectangle in the upper left of each panel gives the rod position. Right column (d),(e),(f): Vertical velocity profiles, averaged over the strip shown shaded in (a), for five values of $v_0$. This strip extends from $r/D = 0.75$ to 1.25. Vertical lines delineate the rod face. Near the surface of the medium ($z \sim 0$), $v_z$ transitions from positive to negative once $\tilde{t} > 1$.

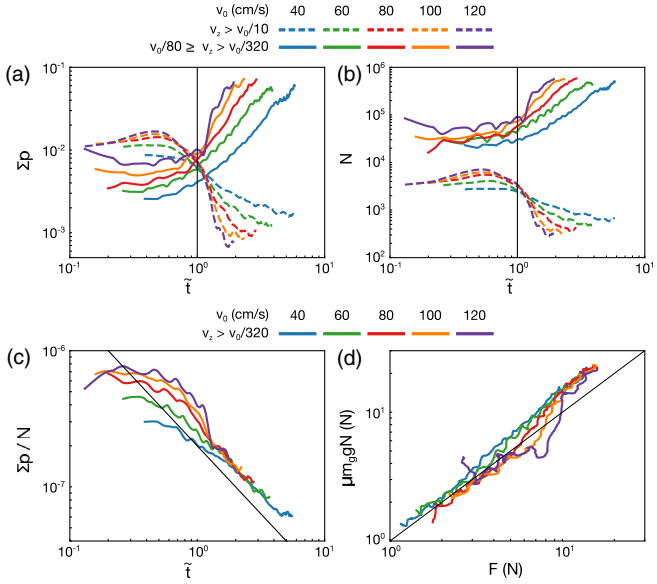


FIG. 5. Simulation results. (a) Summed upward momentum $\sum p$ of all grains at $r > D/2$, binned by vertical velocity magnitude. The momentum carried by the fastest grains ($v_z > v_0/10$, dashed line) decreases sharply at $\tilde{t} = 1$, while increasing for the slowest grains ($v_0/80 \geq v_z > v_0/320$, solid line). (b) The number of grains $N$ in the fastest bin also decreases at $\tilde{t} = 1$, while the number of slow grains grows. (c) The average upward momentum carried per grain decreases throughout the intrusion and collapses onto a $v_0$-independent trend (the line indicates $1/\tilde{t}$) for $\tilde{t} > 1$. (d) Drag force on the rod plotted against the mass of all grains moving with an upward velocity of at least $v_z > v_0/320$ multiplied by the friction coefficient. A 1:1 line is plotted in black.

is carried by the high velocity grains for all $v_0$, but at $\tilde{t} = 1$ a crossover occurs: the net momentum carried by high velocity grains decreases at the same time as that carried by very low velocity grains increases dramatically.

This change is also reflected in the absolute number of high and low velocity grains [Fig. 5(b)]. Though there are more slow than fast grains at all times, as may be expected, at $\tilde{t} = 1$ the disparity begins to grow in the same way as the summed momentum. Indeed, if we plot the average per-grain momentum for all grains with a minimum upward velocity $v_z > v_0/320$, we find that there is velocity dependence only for early times [Fig. 5(c)], correlating with the fluidization of the bed. Once $\tilde{t} = 1$, the average momentum per grain collapses, independently of $v_0$, and decays as $1/\tilde{t}$. This regime is associated with the isolation of the flow around the rod face, seen in Fig. 4(c), especially in the growth of the flow lines as they penetrate into the previously uninvolved bulk grains far away from the rod shaft.

Beyond $\tilde{t} = 1$, the intruder momentum is spread out over a large volume of slow grains [Fig. 4(c) and Fig. 5(c)], foreshadowing the quasistatic character of the resulting drag force. However, we can make this more quantitative. Plotting the force on the intruding rod against the weight of all upward moving grains (taken here as those with magnitude $v_z > v_0/320$) multiplied by $\mu$, to approximate an effective frictional sliding force, yields a strong correlation (Fig. 5d). This agrees with the general aspects of the model proposed by Kang *et al.* [7] for quasi-static drag, who find that the linear $z$-dependence of the drag force results from frictionally engaging an increasing number of particles with depth. Our data extend this by showing that the force on the rod is proportional to the number of engaged particles even in the early, velocity-dependent force region just past the initial peak.

In essence, the entirety of the dynamics are transitioning from inertial to quasistatic behavior: whereas at early times, momentum is carried by localized, high velocity grains, at later times the momentum injected into the system by the intruder is spread out into the bulk and grains move quasistatically. As a result, the velocity dependence of the drag force emerges from a flow field where fluidized grains have easy access to the free surface, and the slight $z$ dependence of the drag (Fig. 3) is due to a

small increase in grains becoming engaged [Fig. 5(b)]. Once the flow field becomes more isolated from the surface due to the gravitational settling of the initially fluidized region, the quickly increasing number of slow-moving grains that must be involved in the motion of the intruder qualitatively changes the nature of the flow and produces the linear increase in drag force with depth. Here we disentangled velocity- and depth-dependent contributions to the drag force on a cylindrical rod by holding the intrusion speed constant. However, given that the cross-over timescale $t^*$ does not depend on speed, we expect the findings to provide a new perspective also for the interpretation and modeling of the many situations where the intruding object comes to rest inside the granular medium.

We thank Kieran Murphy, Melody Lim, and Abhinendra Singh for many helpful discussions, and Paul Umbanhowar for generously lending us glass spheres for this project. This work was supported by the Center for Hierarchical Materials Design (CHiMaD), which is supported by the National Institute of Standards and Technology, U.S. Department of Commerce, under financial assistance Grant No. 70NANB14H012, and by the Army Research Office under Grant No. W911NF-19-1-0245.

*lk.roth.20@gmail.com
†Present address: Center for the Physics of Biological Function, Princeton University, Princeton, New Jersey 08544, USA.
‡h-jaeger@uchicago.edu

[1] A. H. Clark, L. Kondic, and R. P. Behringer, Particle Scale Dynamics in Granular Impact, Phys. Rev. Lett. **109**, 238302 (2012).
[2] D. Bi, S. Henkes, K. E. Daniels, and B. Chakraborty, The statistical physics of athermal materials, Annu. Rev. Condens. Matter Phys. **6**, 63 (2015).
[3] R. C. Hurley, S. A. Hall, J. E. Andrade, and J. Wright, Quantifying Interparticle Forces and Heterogeneity in 3d Granular Materials, Phys. Rev. Lett. **117**, 098005 (2016).
[4] D. van der Meer, Impact on granular beds, Annu. Rev. Fluid Mech. **49**, 463 (2017).
[5] H. Askari and K. Kamrin, Intrusion rheology in grains and other flowable materials, Nat. Mater. **15**, 1274 (2016).
[6] L. Kondic, X. Fang, W. Losert, C. S. O'Hern, and R. P. Behringer, Microstructure evolution during impact on granular matter, Phys. Rev. E **85**, 011305 (2012).
[7] W. Kang, Y. Feng, C. Liu, and R. Blumenfeld, Archimedes law explains penetration of solids into granular media, Nat. Commun. **9**, 1101 (2018).
[8] Y. Feng, R. Blumenfeld, and C. Liu, Support of modified archimedes' law theory in granular media, Soft Matter **15**, 3008 (2019).
[9] C. Li, P. B. Umbanhowar, H. Komsuoglu, D. E. Koditschek, and D. I. Goldman, Sensitive dependence of the motion of a legged robot on granular media, Proc. Natl. Acad. Sci. U.S.A. **106**, 3029 (2009).
[10] M. Omidvar, J. D. Malioche, Z. Chen, M. Iskander, and S. Bless, Visualizing kinematics of dynamic penetration in granular media using transparent soils, Geotechnical testing Journal **38**, 656 (2015).
[11] J. Aguilar and D. I. Goldman, Robophysical study of jumping dynamics on granular media, Nat. Phys. **12**, 278 (2016).
[12] J. Aguilar, T. Zhang, F. Qian, M. Kingsbury, B. McInroe, N. Mazouchova, C. Li, R. Maladen, C. Gong, M. Travers, R. L. Hatton, H. Choset, P. B. Umbanhowar, and D. I. Goldman, A review on locomotion robophysics: The study of movement at the intersection of robotics, soft matter and dynamical systems, Rep. Prog. Phys. **79**, 110001 (2016).
[13] R. Albert, M. A. Pfeifer, A.-L. Barabási, and P. Schiffer, Slow Drag in a Granular Medium, Phys. Rev. Lett. **82**, 205 (1999).
[14] L. Tsimring and D. Volfson, Modeling of impact cratering in granular media, in *Powders and Grains 2005: Proc. 5th Int'l Conf. on Micromechanics of Granular Media, Stuttgart, Germany*, edited by R. Garcia-Rojo, H. J. Herrmann, and S. McNamara (Balkema, Leiden, 2005), pp. 1215–1218, ISBN 0415383471.
[15] H. Katsuragi and D. J. Durian, Unified force law for granular impact cratering, Nat. Phys. **3**, 420 (2007).
[16] D. I. Goldman and P. Umbanhowar, Scaling and dynamics of sphere and disk impact into granular media, Phys. Rev. E **77**, 021308 (2008).
[17] P. Umbanhowar and D. I. Goldman, Granular impact and the critical packing state, Phys. Rev. E **82**, 010301(R) (2010).
[18] A. H. Clark, L. Kondic, and R. P. Behringer, Particle Scale Dynamics in Granular Impact, Phys. Rev. Lett. **109**, 238302 (2012).
[19] A. H. Clark and R. P. Behringer, Granular impact model as an energy-depth relation, Europhys. Lett. **101**, 64001 (2013).
[20] T. A. Brzinski, P. Mayor, and D. J. Durian, Depth-Dependent Resistance of Granular Media to Vertical Penetration, Phys. Rev. Lett. **111**, 168002 (2013).
[21] C. S. Bester and R. P. Behringer, Collisional model of energy dissipation in three-dimensional granular impact, Phys. Rev. E **95**, 032906 (2017).
[22] In addition to the quadratic velocity dependence, there have been suggestions to include a linear term in $F_v$; see, e.g., Ref. [16].
[23] A. Seguin, Y. Bertho, F. Martinez, J. Crassous, and P. Gondret, Experimental velocity fields and forces for a cylinder penetrating into a granular medium, Phys. Rev. E **87**, 012201 (2013).
[24] E. Hamm, F. Tapia, and F. Melo, Dynamics of shear bands in a dense granular material forced by a slowly moving rigid body, Phys. Rev. E **84**, 041304 (2011).
[25] H. Katsuragi and D. J. Durian, Drag force scaling for penetration into granular media, Phys. Rev. E **87**, 052208 (2013).
[26] N. Gravish, P. B. Umbanhowar, and D. I. Goldman, Force and Flow Transition in Plowed Granular Media, Phys. Rev. Lett. **105**, 128301 (2010).
[27] N. Gravish, P. B. Umbanhowar, and D. I. Goldman, Force and flow at the onset of drag in plowed granular media, Phys. Rev. E **89**, 042202 (2014).

[28] G. Caballero, R. Bergmann, D. van der Meer, A. Prosperetti, and D. Lohse, Role of Air in Granular Jet Formation, Phys. Rev. Lett. **99**, 018001 (2007).

[29] J. R. Royer, E. I. Corwin, P. J. Eng, and H. M. Jaeger, Gas-Mediated Impact Dynamics in Fine-Grained Granular Materials, Phys. Rev. Lett. **99**, 038003 (2007).

[30] L. A. Lopez-Rodriguez and F. Pacheco-Vazquez, Friction force regimes and the conditions for endless penetration of an intruder into a granular medium, Phys. Rev. E **96**, 030901 (R) (2017).

[31] S. Plimpton, Fast parallel algorithms for short-range molecular dynamics, J. Comput. Phys. **117**, 1 (1995).

[32] L. K. Roth, Constant speed penetration into granular materials: Drag forces from the quasistatic to inertial regime, Granular Matter **23**, 54 (2021).

[33] L. E. Silbert, D. Ertaş, G. S. Grest, T. C. Halsey, D. Levine, and S. J. Plimpton, Granular flow down an inclined plane: Bagnold scaling and rheology, Phys. Rev. E **64**, 051302 (2001).

[34] See Supplemental Material at http://link.aps.org/supplemental/10.1103/PhysRevLett.126.218001 for a discussion of how the shape of the rod tip affects the initial force peak.

[35] M. Kobayakawa, S. Miyai, T. Tsuji, and T. Tanaka, Local dilation and compaction of granular materials induced by plate drag, Phys. Rev. E **98**, 052907 (2018).